



Interaction between the type 4 pili machinery and a diguanylate cyclase fine-tune c-di-GMP levels during early biofilm formation

Shanice S. Webster^a, Calvin K. Lee^{b,c,d}, William C. Schmidt^{b,c,d}, Gerard C. L. Wong^{b,c,d}, and George A. O'Toole^{a,1}

^aDepartment of Microbiology and Immunology, Geisel School of Medicine at Dartmouth, Hanover, NH 03755; ^bDepartment of Bioengineering, University of California, Los Angeles, CA 90095; ^cDepartment of Chemistry and Biochemistry, University of California, Los Angeles, CA 90095; and ^dCalifornia NanoSystems Institute, University of California, Los Angeles, CA 90095

Edited by Dianne K. Newman, California Institute of Technology, Pasadena, CA, and approved May 19, 2021 (received for review March 24, 2021)

To initiate biofilm formation, it is critical for bacteria to sense a surface and respond precisely to activate downstream components of the biofilm program. Type 4 pili (T4P) and increasing levels of c-di-GMP have been shown to be important for surface sensing and biofilm formation, respectively; however, mechanisms important in modulating the levels of this dinucleotide molecule to define a precise output response are unknown. Here, using macroscopic bulk assays and single-cell tracking analyses of *Pseudomonas aeruginosa*, we uncover a role of the T4P alignment complex protein, PilO, in modulating the activity of the diguanylate cyclase (DGC) SadC. Two-hybrid and bimolecular fluorescence complementation assays, combined with genetic studies, are consistent with a model whereby PilO interacts with SadC and that the PilO–SadC interaction inhibits SadC's activity, resulting in decreased biofilm formation and increased motility. Using single-cell tracking, we monitor both the mean c-di-GMP and the variance of this dinucleotide in individual cells. Mutations that increase PilO–SadC interaction modestly, but significantly, decrease both the average and variance in c-di-GMP levels on a cell-by-cell basis, while mutants that disrupt PilO–SadC interaction increase the mean and variance of c-di-GMP levels. This work is consistent with a model wherein *P. aeruginosa* uses a component of the T4P scaffold to fine-tune the levels of this dinucleotide signal during surface commitment. Finally, given our previous findings linking SadC to the flagellar machinery, we propose that this DGC acts as a bridge to integrate T4P and flagellar-derived input signals during initial surface engagement.

bacterial biofilms | *Pseudomonas aeruginosa* | c-di-GMP | alignment complex | surface sensing

The transition from a planktonic to a biofilm mode of growth is key to the survival of microbes in nature. This switch involves bacteria first sensing surface contact, transmitting that surface signal intracellularly, and finally responding to that signal to activate downstream pathways that lead to biofilm formation (1). While the molecular mechanisms of surface sensing are still unclear, it is well known that the flagella and type 4 pili (T4P) are required not only for detecting surface contact but also for signal transmission (2–7). For example, pioneering work by McCarter and Silverman in 1988 (8, 9), show that decreased rotation of the polar flagellum in *Vibrio parahaemolyticus* upon surface contact initiated a signal transduction pathway that triggered production of lateral flagella. Analogous work in *Pseudomonas aeruginosa* demonstrate that upon surface contact there is increased production of adherent pili (10). In more recent work, the T4P are thought to act as a “force transducer” by detecting the resistance to retraction when cells are surface engaged, thereby activating downstream pathways, such as synthesis of holdfast in *Caulobacter* or activation of the Chp chemosensory (2, 3) and FimS–AlgR two component system (11) in *P. aeruginosa*. In addition to facilitating adhesion and signal transmission, we are now beginning to appreciate the role of these appendages in modulating the levels of second messenger molecules, such as c-di-GMP. For example, Tad pili of *Caulobacter* are

thought to bring the cell pole into close contact with the cell surface upon retraction, such that the flagellar motor can sense surface contact and stimulate c-di-GMP production (12, 13). In *P. aeruginosa*, transcription of genes coding for pili proteins, as well as the localization of PilY1, are needed to up-regulate c-di-GMP levels in a hierarchical signaling cascade (11, 14). The increased c-di-GMP levels, perhaps through a positive feedback mechanism, lead to an increase in T4P production (10).

One defining feature of the T4P machinery is the alignment complex, which is composed of the PilM, PilN, PilO, and PilP proteins (15–17). The alignment complex surrounds the pili fiber and is so called because it forms a bridge between the secretin, PilQ in the outer membrane (OM), and the motor proteins PilB and PilT in the cytoplasm (Fig. 1A). The alignment complex is known for its role in pili assembly and has been shown to functionally contribute to pili extension and retraction, and localization of PilA monomers (18). In a recent study from our group, we provided genetic evidence for role of the T4P alignment complex and PilY1 in up-regulating c-di-GMP as part of a signal transduction cascade involving the diguanylate cyclase (DGC), SadC (11). Based on these findings, we set out to determine the role of these proteins in modulating c-di-GMP levels upon surface engagement.

Based on the present work, our data are consistent with a model whereby, for *P. aeruginosa*, the T4P alignment complex protein, PilO, physically interacts with the DGC SadC, thereby sequestering and decreasing the activity of SadC, which in turn results in increased surface motility and reduced biofilm formation. Using

Significance

Type 4 pili (T4P) of *Pseudomonas aeruginosa* are important for surface sensing and regulating intracellular c-di-GMP levels during biofilm formation. This work supports a role for the T4P alignment complex, previously known for supporting pili biogenesis, in surface-dependent signaling. Our findings indicate that *P. aeruginosa* uses a diguanylate cyclase, via a complex web of protein–protein interactions, to integrate signaling through the T4P and the flagellar motor to fine-tune c-di-GMP levels. A key implication of this work is that more than just regulating signal levels, cells must modulate the dynamic range of c-di-GMP to precisely control the transition to a biofilm lifestyle.

Author contributions: S.S.W., C.K.L., G.C.L.W., and G.A.O. designed research; S.S.W., C.K.L., and W.C.S. performed research; S.S.W. contributed new reagents/analytic tools; S.S.W., C.K.L., W.C.S., G.C.L.W., and G.A.O. analyzed data; and S.S.W., C.K.L., G.C.L.W., and G.A.O. wrote the paper.

The authors declare no competing interest.

This article is a PNAS Direct Submission.

Published under the PNAS license.

¹To whom correspondence may be addressed. Email: georgeo@dartmouth.edu.

This article contains supporting information online at <https://www.pnas.org/lookup/suppl/doi:10.1073/pnas.2105566118/-DCSupplemental>.

Published June 24, 2021.

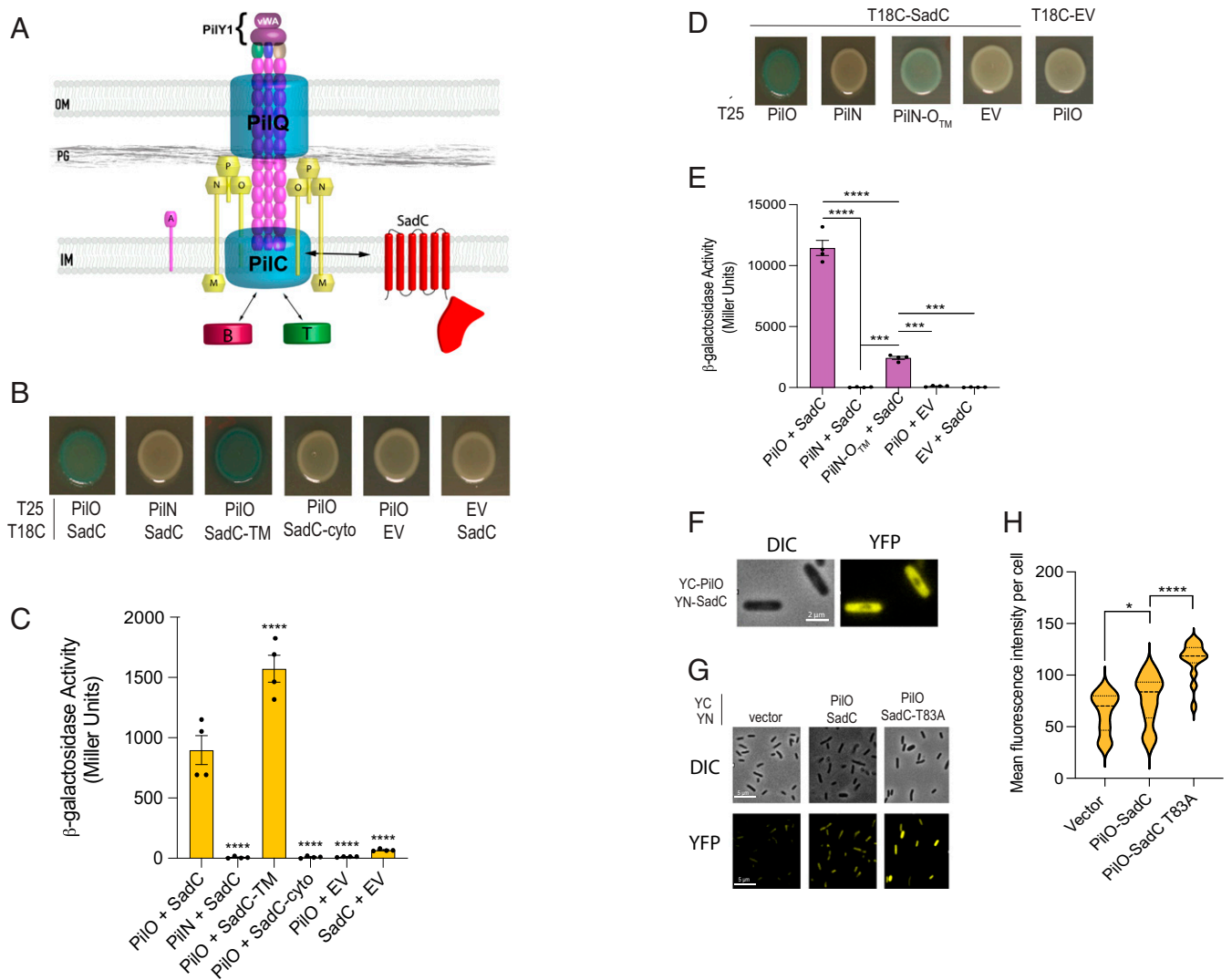


Fig. 1. Diagram of the T4P machinery and the DGC SadC. (A) Shown is a diagram of the T4P machinery illustrating interaction between SadC and PilO, a component of the T4P alignment complex. PG, peptidoglycan. The secretin PilQ and the platform protein PilC are shown in light blue while the pilus fiber, which consists of the major pilin protein PilA (pink) and the minor pilins PilVWX (green, blue and magenta), are also shown. The T4P protein PilY1 consisting of a von Willebrand A (vWA) domain and a C-terminal domain are shown at the tip of the pilus fiber. The extension and retraction ATPases, PilB (magenta), and PilT (green) are also shown. The PilMNOP proteins, which comprise the alignment complex and span the cytoplasm to the OM, are shown in yellow. PilP is present in the periplasm, while PilN and PilO, which are structurally similar, span the periplasm and extend across the IM to the cytoplasm. PilM is localized to the cytoplasm and interacts with PilN. (B) PilO interacts with SadC in the BACTH assay. Images of spots of cotransformations with the indicated proteins fused to the C terminus of the T25 or T18 domains of adenylate cyclase following incubation at 30 °C for 40 h on X-gal-containing agar supplemented with the appropriate antibiotics. Empty vectors (EV) are the negative controls in this and subsequent experiments. (C) β -Galactosidase activity in Miller units for interactions shown in B. (D) Images from the BACTH analysis for SadC cotransformed with PilO, PilN, or PilN-O_{TM} chimera. PilN-O_{TM} is a chimeric protein of PilN with its TMD replaced with that of PilO. Images of spots of cotransformations with the indicated proteins fused to the C terminus of the T25 or T18 domains of adenylate cyclase following incubation at 30 °C for 40 h on X-gal-containing agar supplemented with the appropriate antibiotics, then incubated at 4 °C for an additional 3 d to allow for further color development. Note the difference in incubation times in this panel compared to B. (E) Quantification of β -galactosidase activity of cotransformation from D shown in Miller units. For C and E, β -galactosidase activity was quantified from cells scraped from transformation plates supplemented with antibiotics; the data are from four biological replicates. Error bars show SEM and statistical significance was determined using one-way ANOVA and Dunnett's multiple comparison post hoc test. $***P \leq 0.0001$, $****P \leq 0.0001$. (F) Representative DIC and YFP images for PilO–SadC interaction shown by BiFC analysis. The N terminus of PilO and SadC proteins were fused to the C-terminal (YC) and N-terminal (YN) portions of the YFP, respectively. Note the fluorescence background in the vector. (G) DIC (Upper) and fluorescent (Lower) images from BiFC assay shown for PilO with either empty vector, WT SadC, and SadC-T83A protein variant. The vector is included as the negative control. (H) Quantification of mean fluorescence intensity per cell. Dashed lines on violin plots represent the median and solid lines represent the first and third quartiles. Data points are the mean fluorescence intensity per cell from at least six fields. Data are from three independent experiments performed on different days. P value from a Mann–Whitney U test. $*P \leq 0.05$, $****P \leq 0.0001$.

single-cell tracking, we show that by increasing or decreasing the PilO–SadC interaction, we can modulate the mean and variance of c-di-GMP levels. For example, increasing the PilO–SadC interaction reduces both the mean and c-di-GMP variance among

signaling cells. Our work underscores the role of controlling the output of this dinucleotide signal in a given population via a complex regulatory network. Finally, given the documented role of SadC in interacting with a component of the flagellar motor

(19), we propose a model whereby this DGC can act as a bridge to integrate surface-derived input signals from both the T4P and flagella.

Results

T4P Alignment Complex Protein PilO Physically Interacts with SadC.

We previously reported genetic studies supporting the model that the T4P PilMNOP proteins (i.e., the pilus alignment complex) are involved in signal transduction from the cell surface protein PilY1 to inner membrane (IM)-localized DGC SadC (11) (Fig. 1A); the mechanism underlying this signaling had not been identified. By leveraging the observation that PilY1 protein levels increase when cells are surface-grown, we showed that repression of swarming motility did not occur when PilY1 was overexpressed in the $\Delta pilMNOP$ mutant or for strains carrying single nonpolar mutations in the *pilM*, *pilN*, *pilO*, or *pilP* genes, suggesting a role for the PilMNOP proteins in signaling from PilY1 (11). Similarly, a strain carrying a *sadC* deletion also lost PilY1-dependent swarm suppression (14), implicating the alignment complex and SadC in PilY1-mediated, surface-dependent control of c-di-GMP.

The PilMNOP alignment complex is stabilized by a series of documented protein-protein interactions between PilP-PilN, PilP-PilO, PilN-PilM, and PilN-PilO that span the cytoplasm to the IM of the cell (15, 18). Based on our prior findings and the known interactions among the PilMNOP proteins, we hypothesized that physical interaction between SadC and one or more components of the T4P alignment complex might be important in modulating cellular c-di-GMP levels, which would in turn impact biofilm formation and motility. We focused on PilN and PilO because these proteins share the IM-localization of SadC (15, 18, 20). Using bacterial adenylate cyclase two-hybrid (BACTH) and bimolecular fluorescent complementation (BiFC) studies, we show a significant interaction between PilO and SadC, but not with the structurally similar PilN or other membrane proteins (Fig. 1B and C and *SI Appendix, Fig. S1A and B*), suggesting that the interaction between PilO and SadC is specific.

We next sought to define which portions of SadC and PilO interact. SadC has six predicted membrane helices at its N terminus, constituting a transmembrane domain (TMD) and a C-terminal cytoplasmic GGDEF catalytic domain, while PilO has a single TMD and an extended periplasmic domain (Fig. 1A). We tested interactions between the transmembrane or the cytoplasmic GGDEF domain of SadC with full-length PilO in the BACTH system. PilO interacts with the TMD of SadC, while there was a lack of interaction with the SadC's cytoplasmic catalytic domain (Fig. 1B and C).

Given that PilO has a periplasmic globular head domain and a 22-amino acid α -helix that extends into the IM, we hypothesized that the TMD of PilO is important for interaction with the transmembrane of SadC. To evaluate this prediction, we constructed a chimeric protein with the periplasmic domain of PilN and the TMD of PilO (amino acids 28 to 49), which we designated PilN-PilO_{TM}. BACTH analysis showed significantly more interaction between the PilN-PilO_{TM} chimera and SadC compared to full-length PilN and SadC (albeit, a modest enhancement) (Fig. 1D and E). We did not observe as much interaction with the chimeric protein as we observed for full-length PilO, suggesting that other parts of PilO may be important for interacting with SadC. As additional negative controls, we also tested two known TMD-containing proteins, MotC and PilJ, for interaction with PilO. Our BACTH studies show no interaction between PilO with either MotC or PilJ (*SI Appendix, Fig. S1A*), further supporting the specificity of interaction with SadC.

As a second method to assess the PilO-SadC interaction, we used BiFC. Cells expressing both PilO and SadC fused to the N-terminal and C-terminal halves of the yellow fluorescent protein (YFP) showed a robust fluorescent signal as compared to the vector control (Fig. 1F-H).

We note that the BACTH and BiFC studies are conducted in a heterologous organism (*Escherichia coli*) and, despite using two different experimental systems, we cannot rule out that the observed interactions are due to the expression of these proteins in heterologous systems. We performed the genetic studies in *P. aeruginosa*, described below, to help mitigate this concern.

Likely Surface-Exposed Residues of SadC TMD Modulate Interaction with PilO.

Given that PilO is able to interact with SadC, we hypothesized that mutations in the TMD of SadC could modulate interaction with PilO. To test this hypothesis, we performed BACTH analysis coupled with a genetic screen using error-prone PCR mutagenesis of the TMD of SadC and screened for mutants that affected interaction with PilO. From this screen, we identified two candidate mutations, SadC-T83A and SadC-L172Q. We retested candidates in the BACTH system and found that the SadC-T83A variant increases interaction, while the SadC-L172Q mutant protein disrupts interaction with PilO (Fig. 2A and B and *SI Appendix, Fig. S1B*). BiFC analysis of the SadC-T83A mutant allele showed increased fluorescence as compared to the vector control (Fig. 1G and H), corroborating the results from the BACTH. Steady-state levels of the of the SadC variants were similar to WT and highly enriched in the membrane fraction (*SI Appendix, Fig. S1C and D*).

Using the prediction server Phyre (21), we generated a model of the SadC TMD with an 80% confidence interval based on homology to KdpD, a sensor protein and a member of the two-component regulatory system KdpD/KdpE of *E. coli*. The TMD regions of the KdpD and SadC share 40% sequence identity. The T83 and L172 residues of SadC were mapped to TMD3 and TMD6, respectively, and predicted to be on the surface of the same face of this model (Fig. 2C), suggesting that these surface-exposed, proximal residues of SadC likely both participate in the interaction with PilO.

Mutations in the SadC TMD that Impact Interaction with PilO Have Functional Consequences in *P. aeruginosa*.

To determine if the mutations in SadC that modulate interaction with PilO impact *P. aeruginosa* surface behaviors, we introduced the point mutations onto the chromosome. The SadC-T83A mutant showed reduced c-di-GMP levels, hyperswarmed, and showed decreased biofilm levels as compared to WT (Fig. 2D-F and *SI Appendix, Fig. S2A*). The level of c-di-GMP in the strain expressing the SadC-T83A mutant protein is not significantly different from the $\Delta sadC$ strain (Fig. 2D). Consistent with this observation, the strain expressing the SadC-T83A mutant protein and the $\Delta sadC$ deletion showed the same hyperswarming and reduced biofilm phenotype (Fig. 2E and F and *SI Appendix, Fig. S2A*).

In contrast, the strain carrying the SadC-L172Q mutant protein showed reduced swarming motility (Fig. 2E and F), but a nonsignificant change in global c-di-GMP levels (Fig. 2D) and no significant change in early biofilm formation (*SI Appendix, Fig. S2A*). These data indicate that simply disrupting the PilO-SadC interaction is not sufficient to activate fully SadC, a point we discuss further below.

To test activity of the SadC mutants and to eliminate the possibility that the SadC-T83A mutation negatively affects SadC catalytic activity independent of PilO, we measured c-di-GMP levels of the protein variants in the BACTH system as was previously reported (19). We found that coexpressing SadC variants produced homodimers with comparable levels of c-di-GMP to WT SadC (*SI Appendix, Fig. S3*). For the SadC-T83A mutant there is a slight but nonsignificant decrease in c-di-GMP; this result demonstrates that the SadC-T83A mutation has no significant effect on the catalytic activity of SadC, and that it is the increased interaction with PilO that is responsible for the decreased activity of SadC.

To ensure that the observed phenotypes caused by these mutations in SadC were not due to differences in steady-state protein expression levels, we performed Western blot analysis on FLAG-tagged SadC mutant variants and showed that SadC-T83A and

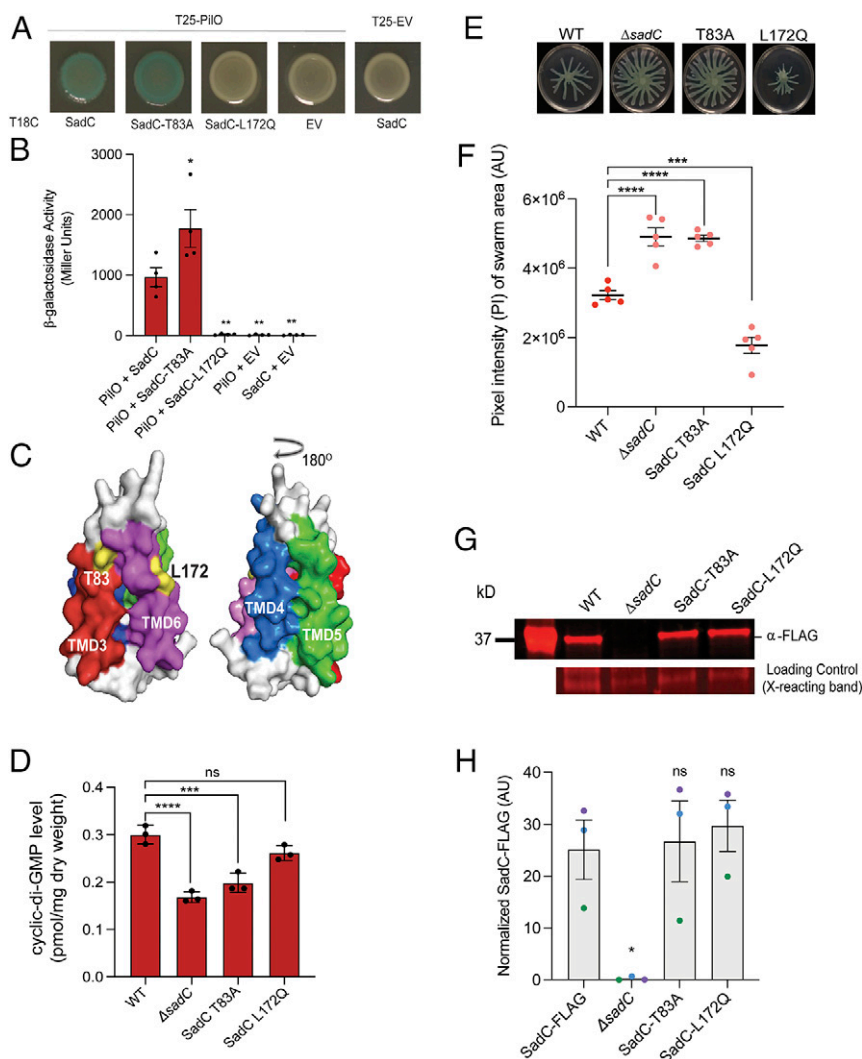


Fig. 2. Mutations in SadC's TMD modulate interaction with PilO and impact c-di-GMP-associated behaviors in *P. aeruginosa*. (A) Images from the BACTH analysis for cotransformations with plasmids expressing PilO and either WT SadC, SadC-T83A, or SadC-L172Q proteins. EV, empty vector. (B) Quantification of β -galactosidase activity in Miller units for interactions in A. Details of experiments and analysis are provided in the legend of Fig. 1. (C) Predicted structure of four of the six N-terminal TMD (amino acids 1 to 187) of SadC. The structure was generated using the prediction software Phyre (21). TMD3 (red), TMD4 (blue), TMD5 (green), and TMD6 (magenta) are shown. Residues T83 and L172 located on TMD3 and TMD6, respectively, are highlighted in yellow. (D) Quantification of global c-di-GMP levels for WT and *sadC* variants. (E) Representative swarm images. (F) Quantification of pixel intensity (PI) of swarm area for images shown in E. Error bars in B, D, and F are SEM and statistical significance was determined by one-way ANOVA and a Dunnett's post hoc test, $*P \leq 0.01$, $***P \leq 0.001$, $****P \leq 0.0001$, and $*****P \leq 0.00001$; ns, not significant. (G) Representative blot for normalized SadC-3xFLAG protein levels. The band at ~30 kDa is a nonspecific, cross-reacting band with the anti-FLAG antibody and serves as an additional loading control. (H) Quantification of normalized SadC-FLAG protein levels of WT and mutants relative to the cross-reacting band. Data are from three biological replicates. Dots with the same color represent the same biological replicate; different colors indicate different biological replicates. Error bars are SEM and statistical significance was determined by one-way ANOVA and a Dunnett's post hoc test. $*P \leq 0.05$; ns, not significant.

SadC-L172Q variants were as stable as WT FLAG-tagged SadC (Fig. 2 G and H). To ensure that FLAG tag was not affecting SadC function, we performed static biofilm assays of FLAG-tagged WT SadC and mutants and found that there was a nonsignificant difference in biofilm levels between WT tagged and untagged SadC. Additionally, FLAG-tagged SadC variants phenocopied untagged SadC mutants (compare *SI Appendix, Fig. S2 A and B*).

These data, together with the BACTH and BiFC analyses, indicate that mutations that increase interaction between PilO and SadC decrease cellular levels of c-di-GMP and suggests a model wherein PilO sequesters SadC and inhibits its activity.

The Small-xxx-Small Motif in the PilO Transmembrane Mediates Interaction with SadC. Given that PilO interacts with SadC via its TMD, we wanted to determine whether there was a specific motif

present in the transmembrane of PilO that might be important for interaction with SadC. We scanned the PilO transmembrane and found that there is a conserved Small-xxx-Small motif present at residues 40 and 44 (A40xxxA44). This motif has been shown to play an important role in helix-helix dimerization in transmembrane proteins (22, 23); thus, we hypothesized that this domain might be mediating interaction between the α -helix of PilO and the SadC TMD. To identify mutations in the A40xxxA44 motif of PilO that impact PilO-SadC interaction, we used two different approaches. First, we generated an E40xxxE44 variant of PilO, but found that this mutant protein was unstable and did not analyze it further (*SI Appendix, Fig. S4*).

As an alternative strategy, we performed a targeted screen wherein we used a primer-based approach to introduce random mutations at amino acid positions 40 and 44 in the PilO-containing

BACTH fragment to generate a mutant library. We then tested the PiLO mutant library for interaction with SadC in the BACTH system and screened for variants of PiLO that increased interaction with SadC, as judged by dark blue colonies in the BACTH assay. We sought mutants that enhanced interaction because we postulated that these alleles were likely to be stable. From this screen, we identified a candidate mutant, PiLO-VxxxL. BACTH studies confirmed that the PiLO-VxxxL mutant protein interacts significantly more strongly with SadC than does the WT PiLO (Fig. 3A). Additionally, PiLO-VxxxL shows similar levels of protein expression and IM localization as WT in whole-cell lysates and IM fractions, respectively (SI Appendix, Fig. S4). Furthermore, the strain expressing the PiLO-VxxxL mutant protein twitches to the same extent as WT, which demonstrates that these mutations do not disrupt the key role of this protein in the T4P alignment complex (SI Appendix, Fig. S5A). We also demonstrated that the PiLO-VxxxL, SadC-T83A, or SadC-L172Q grow as well as the WT strain (SI Appendix, Fig. S6), thus none of the observed phenotypes for these mutants are due to changes in growth of the mutant strains.

Given the findings for the SadC-T83A protein variant that enhance interaction with PiLO results in decreased biofilm formation, hyperswarming, and reduce global c-di-GMP levels, we hypothesized that the PiLO-VxxxL variant would cause similar phenotypic outputs. Surprisingly, however, using bulk assays we did not observe any significant changes in intracellular levels of c-di-GMP, swarming motility, or biofilm formation as compared to WT for the PiLO-VxxxL variant protein (SI Appendix, Fig. S5 B–D).

SadC interacts with both PiLO and MotC, and the interaction between MotC and SadC stimulates SadC's activity (19). Thus, one simple explanation for the lack of bulk phenotypes for the strain carrying the PiLO-VxxxL variant is that despite the increased interaction between SadC and PiLO-VxxxL (which should reduce c-di-GMP level based on our model), SadC's ability to interact with MotC could mitigate the increased PiLO-VxxxL-SadC interaction, thus causing phenotypes to be more subtle. We address the issue of phenotypes for the PiLO-VxxxL mutant directly using single-cell tracking, as described below.

We confirmed the previously reported SadC-MotC interaction (19) and we observed that SadC interacts strongly with MotC (SI Appendix, Fig. S7A), consistent with the idea that PiLO and MotC may be competing for SadC binding. Furthermore, we demonstrated that the SadC-T83A and SadC-L172Q variants still interact with MotC at WT levels (SI Appendix, Fig. S7B). Interestingly, we previously identified the L94 residue of SadC as critical for

interacting with MotC; SadC-L94 is on the same helix as SadC-T83A (Fig. 3B and SI Appendix, Fig. S7C). These data suggest that SadC interacts with PiLO and MotC using the same face of the SadC TMD but via distinct residues on this helix of SadC. To provide additional support that the interaction face on SadC is the same for PiLO and MotC, we generated an α -helical wheel of TMD 3 of SadC. The wheel indeed shows that the T83 residue that mediates interaction with PiLO and the L94 residue, which mediates interaction with MotC, are located next to each other (SI Appendix, Fig. S7C).

Mutations that Modulate Interaction between SadC and PiLO Affect Variation of c-di-GMP Signaling during Biofilm Formation.

Our analysis above is consistent with an interaction between PiLO and SadC, and the interaction between the proteins modulating SadC's DGC activity. As mentioned above, however, some of the macroscopic bulk phenotypes of the strains carrying PiLO mutations were unexpected, being either modest (swarming) or not significantly different from WT (c-di-GMP level and static biofilm formation). To address this issue directly, we used single-cell tracking to investigate changes in c-di-GMP levels during exponential surface colonization by WT and the strains carrying mutant variants of the PiLO and SadC proteins to explore how these mutations might impact c-di-GMP production for populations of cells resolved at the single-cell level.

We tracked single-cell levels of c-di-GMP in the WT and mutant strains using a reporter wherein green fluorescent protein (GFP) was fused to the c-di-GMP-responsive P_{cdrA} promoter, as reported previously (24, 25). After inoculating bacteria into a flow cell, we recorded until the surface was at a cell density that corresponds to roughly when microcolonies begin to form. This density is also when the surface cell count is rising exponentially. In flow cell experiments for *P. aeruginosa*, recording time is generally a poor indicator for the progression of biofilm formation, since most of this time is spent recording a surface where the surface cell density is sparse and roughly constant, and it is extremely difficult to determine a priori how long this period lasts (25–27). Nonetheless, our tracking analysis comprised the first ~40 h after inoculating the flow cell for all strains. In these experiments, we noticed two populations of cells—those expressing and those not expressing GFP—thus, a GFP signal cutoff was defined to partition cells into two subpopulations of c-di-GMP “on” and “off” states (25, 28) (SI Appendix, Fig. S8 and Movie S1). The fraction of c-di-GMP “on” cells in a population is a good measure of whether SadC is active or

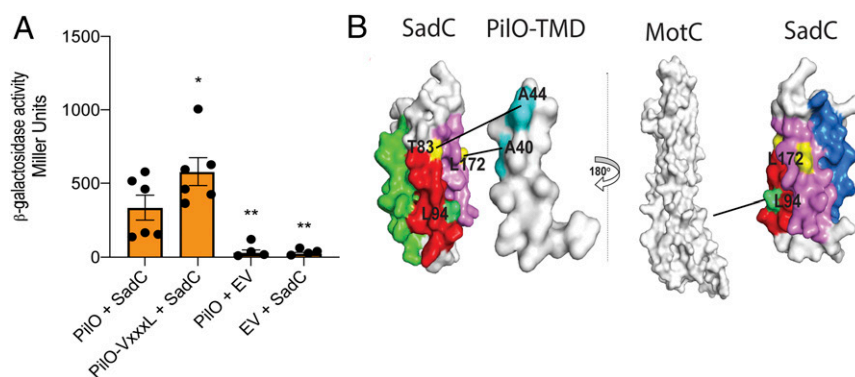


Fig. 3. A conserved Sm-xxx-Sm motif in the TMD of PiLO is important for interaction with SadC. (A) β -Galactosidase activity from the BACTH assay for SadC cotransformed with PiLO or the PiLO-VxxxL mutant protein. EV, empty vector. Dots shown on graph for β -galactosidase assay represent data points from five biological replicates. Error bars are SEM, and statistical significance was determined by a one-way ANOVA and a Dunnett's post hoc test. $*P \leq 0.05$, $**P \leq 0.01$. (B) Surface representation of the structures for SadC, the PiLO-TMD, and MotC determined using Phyre. The helices of the TMD of SadC colored as in Fig. 2 and the SadC-L94P mutation that disrupts interaction with MotC is shown in green, while SadC mutations (T83A and L172Q) that modulate interaction with PiLO are shown in yellow. The PiLO-TMD with the alanine residues of the Sm-xxx-Sm motif are shown in cyan. Rotation of SadC (180°) is shown to better view TMD3 with L172 and L94 residues. The location of SadC-L94P and SadC-T83A on the same face of the α -helix suggests that SadC does not simultaneously interact with both PiLO and MotC.

inactive in those cells, since a c-di-GMP “on” cell should have active SadC producing c-di-GMP, and vice versa. These subpopulations of c-di-GMP “on” and “off” cells have been reported previously in multiple systems (10, 25, 28).

Our data indicate that the PilO–SadC interaction is an important regulatory hub for controlling biofilm formation upon surface contact. We tracked single cells through a single division cycle (from division event to division event) and monitored their c-di-GMP levels as a function of the cell’s lifetime. For each single cell, we can calculate the mean and variance of their c-di-GMP time series signal, which is then plotted for all cells and strains (Fig. 4). The mean and variance data points are then fit to a multivariate Gaussian distribution, of which a contour corresponding to roughly 1 SD of this distribution is marked by the plotted ellipses. These ellipses illustrate the data spread, and the ellipse area overlap (intersection over union) can be used for comparisons between strains (SI Appendix, Table S1). Further comparisons of only the mean or only the variance between strains can be seen in SI Appendix, Fig. S9, and statistically significant differences are computed using the Kruskal–Wallis test followed by the Tukey–Kramer multiple comparisons test (SI Appendix, Tables S2 and S3; significant differences are indicated by red text).

For all strains, the variance in c-di-GMP level has a range of several orders-of-magnitude (note the log scale in Fig. 4). Thus, it appears that this variance in c-di-GMP levels is an inherent feature of the signal itself. Mutations that impact SadC–PilO interactions

or SadC function impact different aspects of c-di-GMP dynamics. For the two mutations that enhance SadC–PilO interactions (SadC-T83A and PilO-VxxxL), we see that the level of c-di-GMP and the cell-to-cell variance of this dinucleotide are reduced compared to the WT (Fig. 4 A and B and SI Appendix, Fig. S9). Compared to that of WT, the ellipses for the two mutants are shifted toward lower values with an overlap of 0.5 (SI Appendix, Table S1), and the mean and variance for the two mutants overlap and are lower, with *P* values of 0.2 (SadC-T83A) and 0.3 (PilO-VxxxL) for the mean (SI Appendix, Table S2) and 0.4 (SadC-T83A) and 0.7 (PilO-VxxxL) for the variance (SI Appendix, Table S3). These data suggest that interactions of SadC and PilO both control the average level and variance in c-di-GMP level on a cell-by-cell basis over time. In contrast, if the *sadC* gene is deleted or if a mutation is introduced that reduces SadC–PilO interaction (SadC-L172Q), we note that the ranges of both the mean and variance in c-di-GMP levels are modestly increased. Both $\Delta sadC$ and SadC-L172Q mutants have their ellipses shifted toward higher values with an overlap of 0.28 compared to SadC-T83A and PilO-VxxxL mutants. Furthermore, the mean and variance in c-di-GMP levels of $\Delta sadC$ and SadC-L172Q mutants are statistically significantly higher than those of SadC-T83A and PilO-VxxxL mutants (*P* < 0.05) (SI Appendix, Tables S2 and S3).

We found that the PilO–SadC interaction strength negatively correlates with both the average and the spread of c-di-GMP levels. For the strains with a larger range of c-di-GMP levels, we also observed a positive Spearman correlation between the mean and

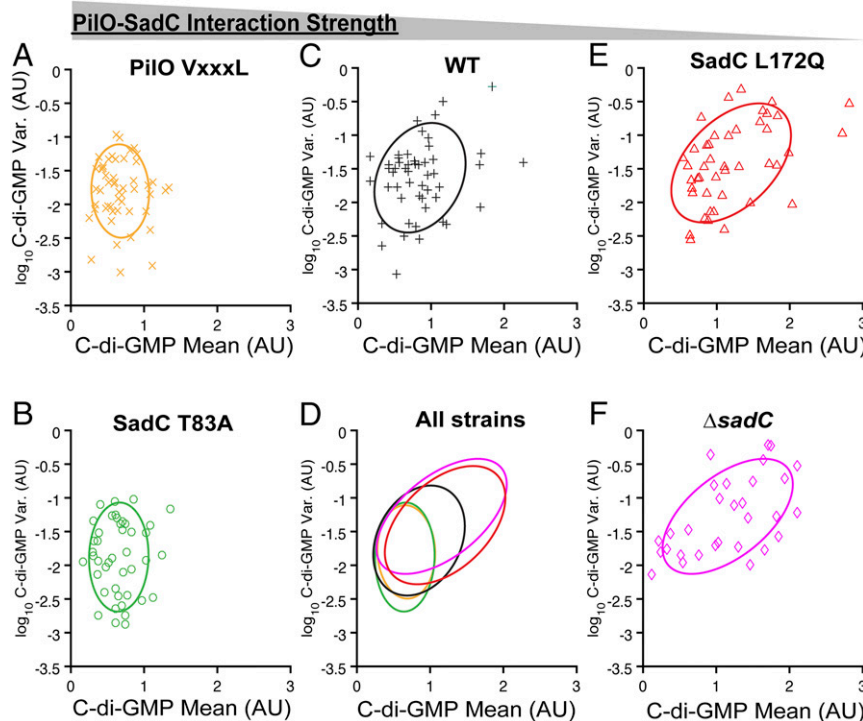


Fig. 4. Single-cell tracking reveals the correlation between PilO–SadC interaction strength and intracellular c-di-GMP. Scatter plots of the mean and variance of c-di-GMP of WT, *sadC*, and *pilO* variants during early biofilm formation. GFP intensity was determined on a cell-by-cell basis for strains carrying the *P_{cdiA}-gfp* construct, a reporter of c-di-GMP levels. Each data point represents one tracked cell through an entire division cycle. The mean and variance characterize the average and spread in c-di-GMP level during the division cycle, respectively. Ellipses are generated from fitting a multivariate Gaussian distribution to the data points, and each ellipse encloses roughly 1 SD of this distribution from the center of mass (centroid) of the points. The size of the ellipse roughly correlates to the range of c-di-GMP levels that the strain can exhibit. The high interaction strength mutants PilO-VxxxL and SadC-T83A (A and B) have the lowest range of the mean and variance of c-di-GMP levels in comparison to WT (C) and the other mutants, while the low interaction strength mutant, SadC-L172Q, has the higher average mean and a wider range of c-di-GMP levels (E). WT sits in the middle of these two scenarios, where its interaction strength, mean, and c-di-GMP variance levels fall between the extremes of these mutants. (F) The null mutant, $\Delta sadC$, shows a pattern similar to the noninteracting, SadC-L172Q mutant variant. A summary plot of all strains using the fitted ellipses is shown in D. The number of data points per strain and the number of cells used to generate the GFP intensities for the mean and variance c-di-GMP calculations for each time point and strain ellipse area overlap between strains, calculated as intersection over union of the ellipse areas, is summarized in SI Appendix, Table S1. The individual axes of the data are shown as violin plots in SI Appendix, Fig. S9, with associated *P* values of multiple comparisons tests summarized in SI Appendix, Tables S2 and S3.

variance (SadC L172Q: 0.487, $P = 9e-4$; $\Delta sadC$: 0.543, $P = 2e-3$), which means that cells with a large average c-di-GMP level also have a large spread in that level. These results suggest that every strain exhibits low and high c-di-GMP levels throughout their time on the surface. PilO–SadC interaction strength is correlated to the time-averaged and maximum c-di-GMP levels that a cell can reach, but all cells will eventually have lower levels regardless of the interaction strength. Observing the changes in c-di-GMP in a cell that we show here is only possible through tracking, since when we only look at single cells in the population grouped by time, these trends are not easily observable.

Discussion

Here, our data are consistent with a model whereby PilO–SadC interaction is important for regulating intracellular c-di-GMP levels and driving early steps biofilm formation. We present three lines of evidence that SadC and PilO interact and that those interactions have a functional consequence. We use BATCH and BiFC to illustrate this interaction. Leveraging the BATCH interaction, we have identified mutations that reduce or enhance the PilO and SadC interaction, and these mutations, when introduced into *P. aeruginosa*, provided complementary information. For one of these mutations, SadC-T83A, we see enhanced interaction between SadC–PilO using both BATCH and BiFC. Mutations that enhance SadC–PilO interaction (e.g., SadC-T83A and PilO-VxxxL) provided similar effects on the single-cell level regarding c-di-GMP mean levels and variance. Similarly, mutations that disrupt SadC–PilO interaction or remove SadC function also have similar single-cell impacts on c-di-GMP. The fact that we observed associations between c-di-GMP mean and variance across a range of levels of this nucleotide and in several different mutant backgrounds suggests that these behaviors are inherent to this signaling system.

Interestingly, the bulk assays with some of these mutants differed from single-cell findings, likely due to the asymmetry of interactions for each protein. That is, PilO interacts with PilN and SadC, while SadC interacts with MotC (which stimulates SadC activity) as well as PilO. This “imbalance” in interactions appears to result in distinct bulk assay phenotypes for the PilO-VxxxL versus the SadC-T83A mutants, despite similar effects on c-di-GMP levels/variance on a cell-by-cell basis. Furthermore, the observation that the PilO-VxxxL impacts swarming motility but not biofilm formation indicates that surface motility may be more sensitive to changes in c-di-GMP levels.

How does this study fit in terms of an overall model for the transition from the planktonic to biofilm state? Based on our findings, we propose that in a planktonic state, PilO interacts with SadC to sequester SadC and inhibit the activity of this DGC. Once cells adhere to a surface, PilO’s interaction with SadC is reduced and the inhibition on SadC is relieved, likely via SadC’s reported interaction with MotC (19), to stimulate and increase cyclic-di-GMP levels (Fig. 5). We do want to highlight potential caveats of our model. For example, as noted in *Results*, the BACTH and BiFC studies are conducted in a heterologous organism (*E. coli*), and despite using two different experimental systems, we cannot rule out that the observed interactions are due to the expression of these proteins in heterologous systems. Thus, we also performed genetic studies in *P. aeruginosa*, using mutations that enhance and reduce interaction between SadC and PilO, as a third line of evidence here to support our conclusions. We note that our original findings using genetic studies indicated that signaling via SadC requires the PilMNOP proteins (11), which comprise the alignment complex. Based on the data here, we cannot rule out alternative mechanistic models that explain these genetic data. For example, the PilMNOP proteins may serve as a scaffold for additional, unidentified components of a signaling complex, and it is such unidentified proteins that are crucial for SadC-dependent signaling. Alternatively, we cannot exclude the possibility that it is the need to functionally assemble the pilus (a known role for the PilMNOP alignment complex proteins)

that is required for SadC-dependent signaling, although we note that in our previous genetic studies, PilA was not required for PilY1-dependent signaling via SadC (11). Thus, additional interaction studies, using pull-downs combined with proteomics analyses, could either strengthen the model presented here or identify other components of a signaling network. We note that such studies will be quite challenging given that SadC is a very low-abundance membrane protein.

There are several possible implications of our findings. First, our work indicates that the T4P alignment complex has dual roles, acting as a scaffold for T4P assembly and as part of an outside-in signal transduction system; the latter would be a novel role for the alignment complex. Second, the observation that SadC can interact with a component of the T4P (PilO) and the flagellar motor (MotC), and both interactions modulate SadC activity to impact surface behaviors like swarming and biofilm formation, indicates that this DGC acts as a bridge to link surface-sensing inputs from these two motility machines. Third, our work highlights the important role of fine-tuning levels of c-di-GMP and maintaining control of signal levels for a population during early biofilm formation. C-di-GMP heterogeneity in *P. aeruginosa* can be driven by the Wsp system, or the phosphodiesterase (PDE) DipA through the c-di-GMP receptor FimW, or through the chemotaxis machinery (10, 25, 28). Our work here shows a variation on this theme, in that SadC’s interactions with PilO and MotC seems to restrict the mean and variance of c-di-GMP levels; disrupting PilO–SadC interactions results in wider range in signal levels that impact surface behaviors. Finally, our data indicate that the population of surface-associated cells can be partitioned into an “on” and “off” state, echoing findings of the Parsek, Jenal, and Miller groups (10, 25, 28). Our data indicate that PilO–SadC interactions impact c-di-GMP heterogeneity and homeostasis in two distinct but complementary ways: switching between c-di-GMP “on” and “off” states as well as controlling the mean/variance in signal levels for actively signaling cells.

We propose that variance in c-di-GMP levels is an inherent feature of the signal itself, analogous to the behaviors we reported previously for cAMP-mediated surface sensing during early biofilm formation (11). The mean and variance of c-di-GMP levels are positively correlated with each other, which implies one of the following scenarios: 1) The cell may be trying to maintain a certain level of the signal through increases/decreases in the production of the signal (via DGC/PDE activity), so it over/undershoots the desired set point as it tries to maintain that set point (like a thermostat). 2) Alternatively, in a cell that has a low (but nonzero) baseline level, the signal spikes and decays (again through DGC/PDE activity) back to baseline level (analogous to neuron activity). In either case, increased DGC activity will result in a greater mean signal, but also a proportionally larger variance in that signal. Similarly, decreased DGC activity will result in the opposite effect. Finally, we expect that modulating the mean, and by extension the variance of the c-di-GMP signal, is only part of the whole picture. The potentially complicated time structure of the c-di-GMP signal (i.e., how fast the signal changes) is another component of the system that we have not investigated here. Furthermore, these c-di-GMP signaling proteins are most likely part of a larger feedback loop network incorporating other DGCs and PDEs. We are essentially perturbing one part of this system (PilO or SadC) and seeing how the changes propagate through the rest of the system, but we have not investigated how the other components of the network (i.e., the other DGCs and PDEs) behave in response to such perturbations. Disentangling such impacts propagated through the system will be challenging.

Our findings raise some interesting questions for future investigation. This work grew out of the observation that surface-dependent stimulation of c-di-GMP by PilY1 requires SadC (11, 29) and the alignment complex (11). Recent work has shown that PilO is highly enriched in PilY1-FLAG pull-downs and cryoelectron tomograph shows that PilY1 likely contacts the alignment complex

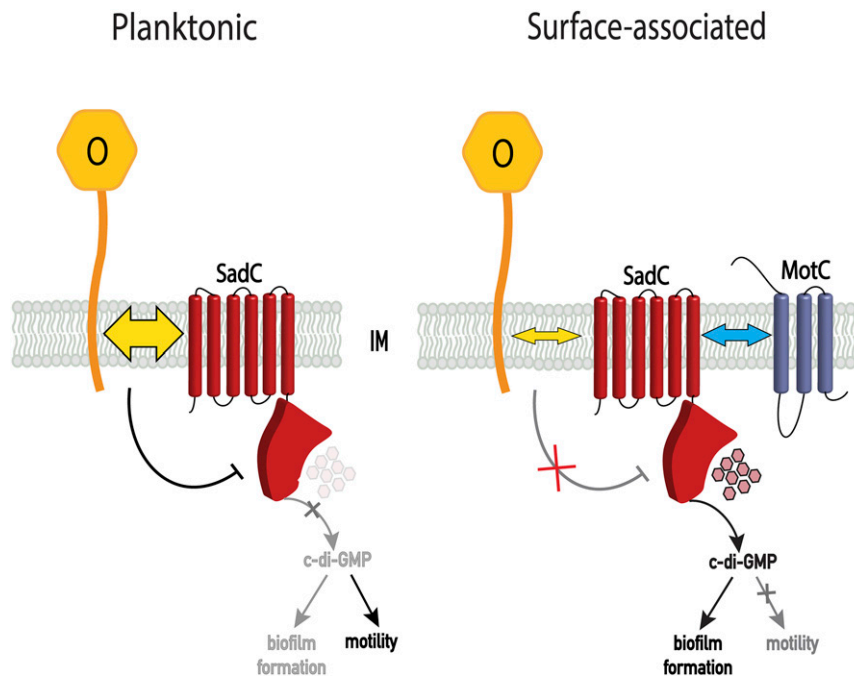


Fig. 5. Proposed model. Proposed model for the role of the PilO–SadC interaction during transition from planktonic to surface-associated or a biofilm state. In a planktonic state, PilO–SadC interaction inhibits SadC’s activity, which results in decreased biofilm formation and increased motility. During surface association, PilO–SadC interaction is disrupted relieving repression of SadC activity; in turn, SadC is stimulated through interaction with MotC. The SadC–MotC interaction results in increased c-di-GMP levels, which promotes biofilm formation and inhibits motility.

via PilO (30), findings consistent with our previous work that PilY1 is likely secreted through the T4P (11). How PilY1 senses surface contact, the role of the putative mechanosensitive von Willibrand A domain in surface sensing, and how the surface-sensing signal is transduced are all open questions.

Materials and Methods

Detailed materials and methods can be found in *SI Appendix, Supplemental Materials and Methods*.

Bacterial Strains, Plasmids, Media, and Growth Conditions. PA14-UCBPP (31) was used as a WT *P. aeruginosa* and *E. coli* 517 was used for chromosomal mutations and BiFC analysis throughout. Strains are listed in *SI Appendix, Table S4*, plasmids are listed in *SI Appendix, Table S5*, and primers are listed in *SI Appendix, Table S6*. All strains were routinely grown in 5 mL lysogeny broth (LB) medium and maintained on 1.5% LB agar plates with appropriate antibiotics, as necessary. Biofilm, swarming, and twitching assays (32–34), as well as flow cells (24, 25, 27) and BACTH assays (35–37) were performed and quantified as reported previously, with additional details outlined in *SI Appendix, Supplemental Materials and Methods*.

Molecular and Biochemical Methods. All in-frame deletions and chromosomal point mutations were generated at the native locus, and plasmid construction (38, 39) and Western blot analysis and quantification (40), subcellular fractionation of proteins (41, 42), protein concentration, and quantification of c-di-GMP (19) were performed as reported previously.

Imaging. Single-cell tracking and quantification was performed as reported previously (25–27). We used the P_{cdrA} -*gfp* reporter (24) to monitor c-di-GMP levels of surface-attached cells.

Data Availability. All study data are included in the article and *SI Appendix*.

ACKNOWLEDGMENTS. We thank Lijun Chen at Michigan State University for mass spectrometry analysis; Lori Burrows for supplying the PilO antibody; Zdenek Svindrych for help with image analysis for BiFC experiments; and the Institute of Biomolecular Targeting (BioMT COBRE) at Dartmouth for providing sequencing, imaging, and protein analysis. The BioMT COBRE is supported by NIH Award P20-GM113132. This work was supported by the NIH via awards R37 AI83256 (to G.A.O.) and R01 AI43730 (to G.C.L.W.). W.C.S. is funded by a NSF Graduate Research Fellowship under DGE-1650604 and DGE-2034835.

1. G. A. O’Toole, G. C. Wong, Sensational biofilms: Surface sensing in bacteria. *Curr. Opin. Microbiol.* **30**, 139–146 (2016).
2. C. K. Ellison *et al.*, Obstruction of pilus retraction stimulates bacterial surface sensing. *Science* **358**, 535–538 (2017).
3. A. Persat, Y. F. Inclan, J. N. Engel, H. A. Stone, Z. Gitai, Type IV pili mechanochemically regulate virulence factors in *Pseudomonas aeruginosa*. *Proc. Natl. Acad. Sci. U.S.A.* **112**, 7563–7568 (2015).
4. A. S. Utada *et al.*, *Vibrio cholerae* use pili and flagella synergistically to effect motility switching and conditional surface attachment. *Nat. Commun.* **5**, 4913 (2014).
5. J. C. Conrad *et al.*, Flagella and pili-mediated near-surface single-cell motility mechanisms in *P. aeruginosa*. *Biophys. J.* **100**, 1608–1616 (2011).
6. M. Schniederberend *et al.*, Modulation of flagellar rotation in surface-attached bacteria: A pathway for rapid surface-sensing after flagellar attachment. *PLoS Pathog.* **15**, e1008149 (2019).
7. M. L. Gibiansky *et al.*, Bacteria use type IV pili to walk upright and detach from surfaces. *Science* **330**, 197 (2010).
8. L. McCarter, M. Hilmen, M. Silverman, Flagellar dynamometer controls swarmer cell differentiation of *V. parahaemolyticus*. *Cell* **54**, 345–351 (1988).
9. L. McCarter, M. Silverman, Surface-induced swarmer cell differentiation of *Vibrio parahaemolyticus*. *Mol. Microbiol.* **4**, 1057–1062 (1990).
10. B. J. Laventie *et al.*, A Surface-induced asymmetric program promotes tissue colonization by *Pseudomonas aeruginosa*. *Cell Host Microbe* **25**, 140–152.e6 (2019).
11. Y. Luo *et al.*, A hierarchical cascade of second messengers regulates *Pseudomonas aeruginosa* surface behaviors. *mBio* **6**, e02456-14 (2015).
12. I. Hug, S. Deshpande, K. S. Sprecher, T. Pfohl, U. Jenal, Second messenger-mediated tactile response by a bacterial rotary motor. *Science* **358**, 531–534 (2017).
13. M. Sangermani, I. Hug, N. Sauter, T. Pfohl, U. Jenal, Tad pili play a dynamic role in *Caulobacter crescentus* surface colonization. *mBio* **10**, e01237-19 (2019).
14. S. L. Kuchma *et al.*, Cyclic-di-GMP-mediated repression of swarming motility by *Pseudomonas aeruginosa*: The *pilY1* gene and its impact on surface-associated behaviors. *J. Bacteriol.* **192**, 2950–2964 (2010).
15. T. L. Leighton, N. Dayalani, L. M. Sampaleanu, P. L. Howell, L. L. Burrows, Novel role for PilNO in Type IV pilus retraction revealed by alignment subcomplex mutations. *J. Bacteriol.* **197**, 2229–2238 (2015).
16. M. Ayers *et al.*, PilM/N/O/P proteins form an inner membrane complex that affects the stability of the *Pseudomonas aeruginosa* type IV pilus secretin. *J. Mol. Biol.* **394**, 128–142 (2009).

17. S. Tammam *et al.*, Characterization of the PilN, PilO and PilP type IVa pilus sub-complex. *Mol. Microbiol.* **82**, 1496–1514 (2011).
18. S. Tammam *et al.*, PilMNOPQ from the *Pseudomonas aeruginosa* type IV pilus system form a transenvelope protein interaction network that interacts with PilA. *J. Bacteriol.* **195**, 2126–2135 (2013).
19. A. E. Baker *et al.*, Flagellar stators stimulate c-di-GMP production by *Pseudomonas aeruginosa*. *J. Bacteriol.* **201**, e00741-18 (2019).
20. B. Zhu *et al.*, Membrane association of SadC enhances its diguanylate cyclase activity to control exopolysaccharides synthesis and biofilm formation in *Pseudomonas aeruginosa*. *Environ. Microbiol.* **18**, 3440–3452 (2016).
21. L. A. Kelley, S. Mezulis, C. M. Yates, M. N. Wass, M. J. Sternberg, The Phyre2 web portal for protein modeling, prediction and analysis. *Nat. Protoc.* **10**, 845–858 (2015).
22. K. C. Mudumbi, A. Julius, J. Herrmann, E. Li, The pathogenic A391E mutation in FGFR3 induces a structural change in the transmembrane domain dimer. *J. Membr. Biol.* **246**, 487–493 (2013).
23. E. Li, W. C. Wimley, K. Hristova, Transmembrane helix dimerization: Beyond the search for sequence motifs. *Biochim. Biophys. Acta* **1818**, 183–193 (2012).
24. M. T. Rybtke *et al.*, Fluorescence-based reporter for gauging cyclic di-GMP levels in *Pseudomonas aeruginosa*. *Appl. Environ. Microbiol.* **78**, 5060–5069 (2012).
25. C. R. Armbruster *et al.*, Heterogeneity in surface sensing suggests a division of labor in *Pseudomonas aeruginosa* populations. *eLife* **8**, e45084 (2019).
26. C. K. Lee *et al.*, Multigenerational memory and adaptive adhesion in early bacterial biofilm communities. *Proc. Natl. Acad. Sci. U.S.A.* **115**, 4471–4476 (2018).
27. C. K. Lee *et al.*, Social cooperativity of bacteria during reversible surface attachment in young biofilms: A quantitative comparison of *Pseudomonas aeruginosa* PA14 and PAO1. *mBio* **11**, e02644-19 (2020).
28. B. R. Kulasekara *et al.*, c-di-GMP heterogeneity is generated by the chemotaxis machinery to regulate flagellar motility. *eLife* **2**, e01402 (2013).
29. S. L. Kuchma, E. F. Griffin, G. A. O'Toole, Minor pilins of the type IV pilus system participate in the negative regulation of swarming motility. *J. Bacteriol.* **194**, 5388–5403 (2012).
30. A. Treuner-Lange *et al.*, PilY1 and minor pilins form a complex priming the type IVa pilus in *Myxococcus xanthus*. *Nat. Commun.* **11**, 5054 (2020).
31. L. G. Rahme *et al.*, Common virulence factors for bacterial pathogenicity in plants and animals. *Science* **268**, 1899–1902 (1995).
32. D. G. Ha, S. L. Kuchma, G. A. O'Toole, Plate-based assay for swarming motility in *Pseudomonas aeruginosa*. *Methods Mol. Biol.* **1149**, 67–72 (2014).
33. G. A. O'Toole, Microtiter dish biofilm formation assay. *J. Vis. Exp.* **47**, 2437 (2011).
34. G. A. O'Toole, R. Kolter, Flagellar and twitching motility are necessary for *Pseudomonas aeruginosa* biofilm development. *Mol. Microbiol.* **30**, 295–304 (1998).
35. G. Karimova, J. Pidoux, A. Ullmann, D. Ladant, A bacterial two-hybrid system based on a reconstituted signal transduction pathway. *Proc. Natl. Acad. Sci. U.S.A.* **95**, 5752–5756 (1998).
36. J. H. Miller, *A Short Course in Bacterial Genetics* (Cold Spring Harbor Press, 1992).
37. S.T. Smale, Beta-galactosidase assay. *Cold Spring Harb. Protoc.* **2010**, pdb prot5423 (2010).
38. K. H. Choi, A. Kumar, H. P. Schweizer, A 10-min method for preparation of highly electrocompetent *Pseudomonas aeruginosa* cells: Application for DNA fragment transfer between chromosomes and plasmid transformation. *J. Microbiol. Methods* **64**, 391–397 (2006).
39. J. Bachman, Site-directed mutagenesis. *Methods Enzymol.* **529**, 241–248 (2013).
40. M. M. Bradford, A rapid and sensitive method for the quantitation of microgram quantities of protein utilizing the principle of protein-dye binding. *Anal. Biochem.* **72**, 248–254 (1976).
41. D. N. Nunn, S. Lory, Cleavage, methylation, and localization of the *Pseudomonas aeruginosa* export proteins XcpT, -U, -V, and -W. *J. Bacteriol.* **175**, 4375–4382 (1993).
42. S. M. Hinsa, G. A. O'Toole, Biofilm formation by *Pseudomonas fluorescens* WCS365: A role for LapD. *Microbiology (Reading)* **152**, 1375–1383 (2006).